Molecular dynamics simulation of amphiphilic molecules in solution: Micelle formation and dynamic coexistence

Susumu Fujiwara,[1,a)] Takashi Itoh,[1] Masato Hashimoto,[1] and Ritoku Horiuchi[2]
[1]*Department of Macromolecular Science and Engineering, Graduate School of Science and Technology, Kyoto Institute of Technology, Matsugasaki, Sakyo-ku, Kyoto 606-8585, Japan*
[2]*Department of Simulation Science, National Institute for Fusion Science, 322-6 Oroshi-cho, Toki-shi 509-5292, Japan*

(Received 12 November 2008; accepted 16 January 2009; published online 8 April 2009)

The micelle formation and the dynamic coexistence in amphiphilic solution are investigated by molecular dynamics simulation of coarse-grained rigid amphiphilic molecules with explicit solvent molecules. Our simulations show that three kinds of isolated micelles (disk, cylindrical, and spherical micelles) are observed at a lower temperature by quenching from a random configuration of amphiphilic molecules in solution at a higher temperature. The micellar shape changes from a disk into a cylinder, and then into a sphere as the hydrophilic interaction increases whereas it is not so sensitive to the variation of the hydrophobic interaction. This fact indicates that the hydrophilic interaction plays an important role in determining the micellar shape in the range of the interaction parameters used. It is also found that in a certain interaction parameter range, two kinds of micellar shapes coexist dynamically. From the detailed analyses of the dynamic coexistence, it is ascertained that the dynamic coexistence of a cylindrical micelle and a spherical micelle accompanies the coalescence and fragmentation of micelles while that of a disk micelle and a cylindrical micelle does not, but exhibits the continuous change between them. © *2009 American Institute of Physics*.
[DOI: 10.1063/1.3105341]

I. INTRODUCTION

In aqueous solutions, amphiphilic molecules such as lipids, surfactants, and block copolymers spontaneously self-assemble into a wide variety of structures ranging from micelles and bilayers to bicontinuous cubic structures.[1–3] These structures can transform from one to another by changing the solution conditions such as concentration, temperature, and other physicochemical parameters. Such self-assembly phenomena of amphiphilic molecules are of principal importance in many biological and industrial processes. Surfactants have a wide range of important applications in the pharmaceutical, cosmetics and textile industries. Recently, self-assembled bolaamphiphile nanotubes have been used as templates to produce metal-coated nanowires.[4] Investigation of the self-assembling nature of amphiphilic molecules is essential to control such nanometer-sized structures. However, the initial process of self-assembly and the transient intermediate structures formed during the transition between two equilibrium phases have received little attention until recently due to the experimental difficulties. Millisecond time-resolved small-angle x-ray scattering study has revealed the transient states in the formation of unilamellar vesicles only recently.[5]

The method of molecular simulations is very useful in investigating not only the static properties but also the dynamical properties of amphiphilic molecules. Over the last two decades, many simulation studies have been done in relation to the self-assembly of amphiphilic molecules.[6–25] Smit *et al.*[6,7] carried out molecular dynamics (MD) simulations of the spontaneous aggregation of surfactants for a simple oil/water/surfactant system and analyzed the detailed structure of a water/oil interface in the presence of micelles. MD simulations of coarse-grained amphiphilic molecules in solution were performed by Goetz *et al.*[10,11] in order to investigate the spontaneous self-assembly of amphiphilic molecules into spherical micelles, cylindrical micelles, and bilayers. Marrink *et al.*[12] studied the kinetics of spontaneous micelle formation by means of MD simulations of surfactant molecules in water. In these two studies,[10–12] the formed cylindrical micelles and bilayers were not isolated but periodically connected ones without edges. The self-assembly and fusion dynamics of vesicles were studied by Noguchi *et al.*[13,14] using a Brownian dynamics simulation of simplified amphiphilic molecules without solvent. Dissipative particle dynamics simulations were also performed to investigate the phase behavior of amphiphilic solution,[16,17] budding and fission dynamics of two-component vesicles,[18] and spontaneous self-assembly process for threadlike micelles.[19] Klein and co-workers[20–22] proposed several approaches to build coarse-grained models for aqueous surfactants. Several investigations on the dynamics of micellar fusion and fission have recently been made.[23–25] Although simulation studies on the dynamics of amphiphilic molecules in solution have thus been done intensively, little is known about the detailed mechanism of micelle formation in amphiphilic solution at the molecular level. In particular, the formation processes of the *isolated* cylindrical micelles and bilayers with edges have not so far been analyzed in detail.

[a)]Electronic mail: fujiwara@kit.ac.jp. URL: http://www.cis.kit.ac.jp/~fujiwara/.

The purpose of this paper is to clarify the molecular mechanism of micelle formation in amphiphilic solution. Our particular concern is to investigate how the micellar shape changes depending on the hydrophilicity and hydrophobicity. With a view to investigating the self-assembling processes of amphiphilic molecules in solution *at the molecular level*, we carry out the MD simulations of coarse-grained amphiphilic molecules with explicit solvent molecules and analyze the dynamical processes of micelle formation systematically. The molecular mobility and the micellar shape change will be discussed in the subsequent paper.[26]

This paper is organized as follows. In Sec. II we describe the concept of opposing force[1,2,27] and explain in detail our simulation model and method. Our simulation results and discussion on the micelle formation and the dynamic coexistence are presented in Sec. III. In Sec. IV conclusions are given.

II. SIMULATION MODEL AND METHOD

Before explaining our simulation model and method, we should describe the concept of opposing forces which was originally proposed by Tanford.[1,2,27] The major forces that govern the self-assembly of amphiphilic molecules are the hydrophobic attraction at the hydrocarbon-water interface and the hydrophilic repulsion of the head groups. The former attractive interaction arises mainly from the interfacial tension forces at the hydrocarbon-water interface. On the other hand, the latter repulsive interaction includes several contributions such as a steric contribution, a hydration contribution and an electrostatic contribution.

The computational model is the same as that used in the previous work,[28,29] which is based on the models of Goetz *et al.*[10,11] and Noguchi *et al.*[13,14] An amphiphilic molecule is a rigid rod which consists of one hydrophilic particle and two hydrophobic particles. A solvent molecule is modeled as a hydrophilic particle. The mass of each particle is m. The interaction between a hydrophilic particle and a hydrophobic particle is modeled by a repulsive soft core potential,

$$U_{\mathrm{SC}}(r) = 4\varepsilon_{\mathrm{SC}}\left(\frac{\sigma_{\mathrm{SC}}}{r}\right)^9, \tag{1}$$

the interaction between a hydrophilic head particle and a solvent particle is modeled by a Lennard-Jones potential,

$$U_{\mathrm{LJ}}^{\mathrm{hs}}(r) = 4\varepsilon_{\mathrm{hs}}\left[\left(\frac{\sigma}{r}\right)^{12} - \left(\frac{\sigma}{r}\right)^6\right], \tag{2}$$

and all other interactions are modeled by a Lennard-Jones potential,

$$U_{\mathrm{LJ}}(r) = 4\varepsilon\left[\left(\frac{\sigma}{r}\right)^{12} - \left(\frac{\sigma}{r}\right)^6\right], \tag{3}$$

where r is the interparticle distance, $\varepsilon_{\mathrm{SC}}$ is an interaction parameter for the intensity of the hydrophobic interaction, and $\varepsilon_{\mathrm{hs}}$ is that for the intensity of the hydrophilic interaction. The parameter σ_{SC} is set to be $\sigma_{\mathrm{SC}}=1.05\sigma$ as in Ref. 10 and the cutoff distance for these potentials is $r_c=3.0\sigma$. We use the shifted force variant of these potentials,

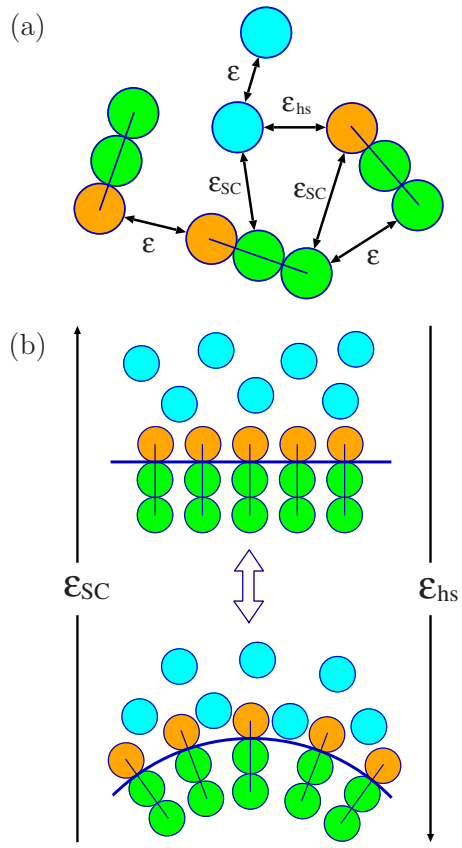

FIG. 1. (Color online) Schematic illustration of (a) the interaction parameters: $\varepsilon_{\mathrm{SC}}$, $\varepsilon_{\mathrm{hs}}$, and ε and (b) the effects of the hydrophobic attraction ($\varepsilon_{\mathrm{SC}}$) and the hydrophilic repulsion ($\varepsilon_{\mathrm{hs}}$) on the interfacial curvature. Dark gray (or orange color), gray (or green color), and light gray (or light blue color) denote the hydrophilic head particles, the hydrophobic tail particles, and the solvent particles, respectively. The curvature of the tail-solvent interface (thick line) tends to become larger with the decrease of $\varepsilon_{\mathrm{SC}}$ or with the increase of $\varepsilon_{\mathrm{hs}}$.

$$V(r) = U(r) - U(r_c) - \left.\frac{\partial U}{\partial r}\right|_{r=r_c}(r - r_c), \tag{4}$$

in order to avoid discontinuities both in the potential energy and in the force. In our simulation model, the intensity of the hydrophobic attraction and the hydrophilic repulsion can be controlled by the interaction parameters between the hydrophilic particles and the tail particles ($\varepsilon_{\mathrm{SC}}$) and those between the head particles and the solvent particles ($\varepsilon_{\mathrm{hs}}$), respectively. We show, in Fig. 1, the schematic illustration of the interaction parameters ($\varepsilon_{\mathrm{SC}}$, $\varepsilon_{\mathrm{hs}}$, and ε) and the effects of the hydrophobic attraction ($\varepsilon_{\mathrm{SC}}$) and the hydrophilic repulsion ($\varepsilon_{\mathrm{hs}}$) on the curvature of the tail-solvent interface. As $\varepsilon_{\mathrm{SC}}$ decreases or $\varepsilon_{\mathrm{hs}}$ increases, the interfacial curvature tends to increase.

In what follows, we represent dimensionless quantities by an asterisk, e.g., energy $\varepsilon_{\mathrm{hs}}^*=\varepsilon_{\mathrm{hs}}/\varepsilon$, number density $\rho^*=\rho\sigma^3$, time $t^*=t\sqrt{\varepsilon/m\sigma^2}$ and temperature $T^*=k_BT/\varepsilon$, where k_B is the Boltzmann constant. The equations of motion for all particles are solved numerically using the leap-frog algorithm at constant temperature ($T^*=1.3$) with a time step of $\Delta t^*=0.0025$ and the temperature is controlled at every 10 time steps by *ad hoc* velocity scaling.[30] We apply the peri-

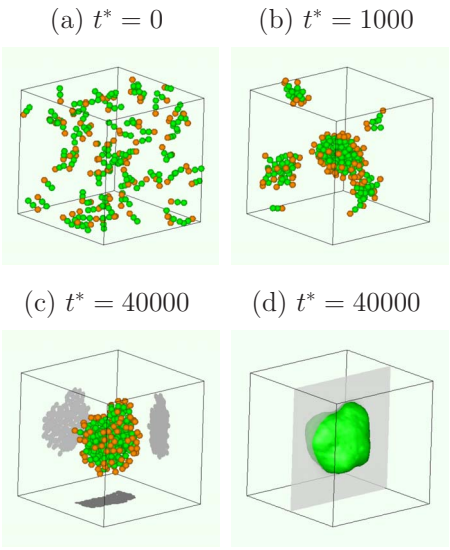

FIG. 2. (Color online) Snapshots of the self-assembly process for $(\varepsilon^*_{SC}, \varepsilon^*_{hs})=(1.0, 1.0)$: (a) $t^*=0$, (b) $t^*=1000$, and (c), (d) $t^*=40\,000$. The self-assembled structure formed in this process is a disk micelle. In (c) and (d), gray shadows of the disk micelle projected on three planes and an isosurface of tail particles are, respectively, depicted to make the micellar shape understandable. The isosurface is calculated by Gaussian splatting techniques. Dark gray (or orange color) and light gray (or green color) particles denote hydrophilic head particles and hydrophobic tail particles, respectively. Note that solvent molecules are not displayed for clarity.

odic boundary conditions and the number density is set to $\rho^*=0.75$.

The MD simulations are performed in the following way. At first, we provide a randomly distributed configuration of 97 amphiphilic molecules immersed in a bath of solvent particles at high temperature ($T^*=10$) for various values of the interaction parameters ε^*_{SC} and ε^*_{hs} $(1.0 \le \varepsilon^*_{SC},\ \varepsilon^*_{hs} \le 4.0)$. The number of solvent particles is 5541, which leads to the amphiphilic concentration of 0.05 and the side length for the cubic simulation box of 19.8. The system is then quenched to $T^*=1.3$ and MD simulations of $t^*=4.0\times10^4$ $(1.6\times10^7$ time steps) are carried out for each simulation run typically. In Sec. III, we study the micelle formation process and the dynamic coexistence of micellar shapes in detail.

III. SIMULATION RESULTS AND DISCUSSION

A. Micelle formation

1. Spontaneous aggregation into micelles

In order to see the micelle formation process, we show, in Fig. 2, the snapshots of the spontaneous aggregation process at various times ($t^*=0$, 1000, and 40 000) for $(\varepsilon^*_{SC}, \varepsilon^*_{hs})=(1.0, 1.0)$. Gray shadows of the amphiphilic molecules projected on three planes and an isosurface of tail particles, which is calculated by Gaussian splatting techniques, are depicted in Figs. 2(c) and 2(d), respectively, to show the micellar shape clearly. Note that solvent molecules are not depicted in this figure. We find the following features from Fig. 2: (i) At the initial time ($t^*=0$), the configuration of the amphiphilic molecules is *random* and almost all the amphiphilic molecules are *isolated*. (ii) As time elapses, small micelles are formed in several positions ($t^*=1000$). (iii) Several small micelles then coalesce into a large micelle and the

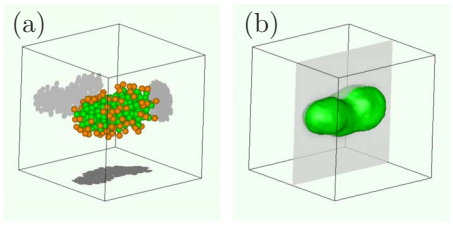

FIG. 3. (Color online) Snapshots of the cylindrical micelle formed by amphiphilic molecules at $t^*=40\,000$ for $(\varepsilon^*_{SC}, \varepsilon^*_{hs})=(1.0, 2.0)$. In (a) and (b), gray shadows of the cylindrical micelle projected on three planes and an isosurface of tail particles, respectively, are also depicted to make the micellar shape understandable. Dark gray (or orange color) and light gray (or green color) particles denote hydrophilic head particles and hydrophobic tail particles, respectively. Note that solvent molecules are not displayed for clarity.

disk micelle is finally formed ($t^*=40\,000$). We show, in Figs. 3 and 4, the snapshots of micelles formed by amphiphilic molecules for $(\varepsilon^*_{SC}, \varepsilon^*_{hs})=(1.0, 2.0)$ and (1.0, 4.0), respectively. Isosurfaces of tail particles are depicted also in these figures. Figures 3 and 4 tell us that the micellar structure formed for $(\varepsilon^*_{SC}, \varepsilon^*_{hs})=(1.0, 2.0)$ is *cylindrical* and that for $(\varepsilon^*_{SC}, \varepsilon^*_{hs})=(1.0, 4.0)$ is almost *spherical*. As can be seen in Figs. 2–4, three kinds of micellar shapes (disk, cylinder, and sphere) appear in our simulation. The dependence of the micellar shape on the intensity of the hydrophilic or hydrophobic interaction will be analyzed more elaborately in Sec. III A 4. Our simulations also indicate that the micellar shape changes from a disk into a cylinder, and then into a sphere as the intensity of the hydrophilicity (ε^*_{hs}) increases. The snapshots of micelles formed for $(\varepsilon^*_{SC}, \varepsilon^*_{hs})=(2.0, 1.0)$ and (3.0, 1.0) indicate that only disk micelle can be observed for large values of ε^*_{SC} (figure not shown). These facts suggest that the micellar shape depends primarily on the hydrophilicity in our interaction parameter range.

2. Potential energy

Here, we examine the energy relaxation during the micelle formation process. We show, in Fig. 5, the time dependence of the total potential energy for $(\varepsilon^*_{SC}, \varepsilon^*_{hs})=(1.0, 4.0)$, (1.0, 1.0), and (3.0, 1.0). This figure indicates that, more or less, potential energies relax *in a stepwise manner*. We also find that such stepwise nature is enhanced as the intensity of the hydrophilicity (ε^*_{hs}) decreases [Figs. 5(a) and 5(b)] or that of the hydrophobicity (ε^*_{SC}) increases [Figs. 5(b) and 5(c)].

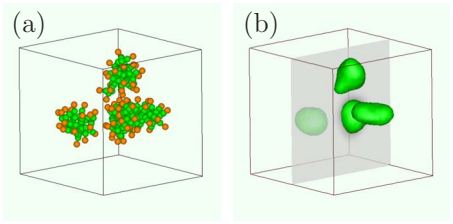

FIG. 4. (Color online) Snapshots of the spherical micelles formed by amphiphilic molecules at $t^*=28\,000$ for $(\varepsilon^*_{SC}, \varepsilon^*_{hs})=(1.0, 4.0)$. In (b), an isosurface of tail particles is also depicted to make the micellar shape understandable. Dark gray (or orange color) and light gray (or green color) particles denote hydrophilic head particles and hydrophobic tail particles, respectively. Note that solvent molecules are not displayed for clarity.

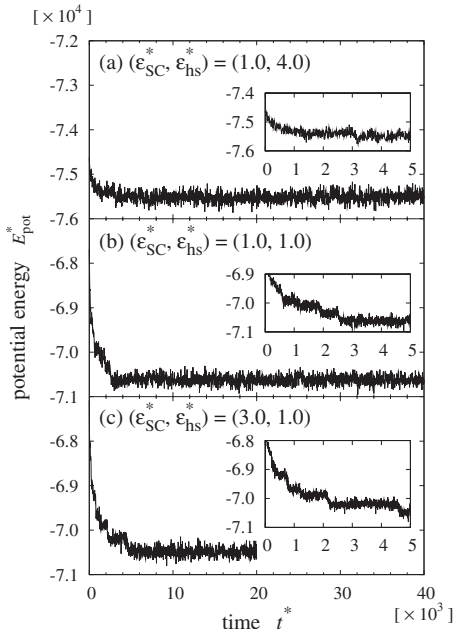

FIG. 5. The total potential energy E_{pot} vs time t (a) for $(\varepsilon^*_{\mathrm{SC}},\varepsilon^*_{\mathrm{hs}})=(1.0,4.0)$, (b) for $(\varepsilon^*_{\mathrm{SC}},\varepsilon^*_{\mathrm{hs}})=(1.0,1.0)$, and (c) for $(\varepsilon^*_{\mathrm{SC}},\varepsilon^*_{\mathrm{hs}})=(3.0,1.0)$. The insets show magnified views in the short time region.

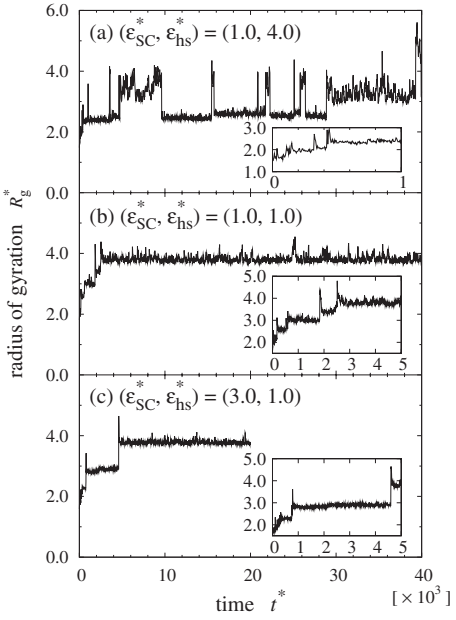

FIG. 6. The radius of gyration R_g versus time t (a) for $(\varepsilon^*_{\mathrm{SC}},\varepsilon^*_{\mathrm{hs}})=(1.0,4.0)$, (b) for $(\varepsilon^*_{\mathrm{SC}},\varepsilon^*_{\mathrm{hs}})=(1.0,1.0)$, and (c) for $(\varepsilon^*_{\mathrm{SC}},\varepsilon^*_{\mathrm{hs}})=(3.0,1.0)$. The insets show magnified views in the short time region.

This observation can be interpreted in the following way. In the case of small hydrophilicity $(\varepsilon^*_{\mathrm{hs}})$ or large hydrophobicity $(\varepsilon^*_{\mathrm{SC}})$, the energy gain due to the coalescence of micelles becomes large since the cohesive energy by amphiphilic molecules increases as $\varepsilon^*_{\mathrm{hs}}$ decreases or $\varepsilon^*_{\mathrm{SC}}$ increases. This large energy gain by the coalescence of micelles for small $\varepsilon^*_{\mathrm{hs}}$ or large $\varepsilon^*_{\mathrm{SC}}$ causes the enhancement of the stepwise nature of the total potential energy.

3. Radius of gyration

In order to investigate the micelle formation process at the molecular level, we define a *micelle* as a collection of amphiphilic molecules whose tail particles are located close to each other.[7] A micelle is precisely defined in the following way. Two amphiphilic molecules, i and j, belong to the same micelle if the following condition is satisfied: $\min_{k,l}|\mathbf{r}^i_k-\mathbf{r}^j_l|<r_0$, where $\mathbf{r}^i_k$ is the position vector of the kth tail particle in the ith amphiphilic molecule. In our calculations, we set $r_0=1.4\sigma$. In Fig. 6, we show the radius of gyration R^*_g of the largest micelle as a function of time for $(\varepsilon^*_{\mathrm{SC}},\varepsilon^*_{\mathrm{hs}})=(1.0,4.0)$, (1.0, 1.0), and (3.0, 1.0). As can be seen in this figure, R^*_g is found to increase in a stepwise manner in connection with the energy relaxation [Fig. 5] in the course of the initial micelle formation process. Sharp bumps are observed when such stepwise increases of R^*_g occur, which implies that the micelle formation proceeds through the coalescence of smaller micelles. We also find that the increases or decreases occur repeatedly in the case of large values of $\varepsilon^*_{\mathrm{hs}}$ [Fig. 6(a)], which means that the coalescence and fragmentation of micelles occur frequently for large hydrophilicity $(\varepsilon^*_{\mathrm{hs}})$.

4. Micellar shape distribution

In this subsection, we examine the micellar shape distribution in order to investigate quantitatively how the micellar shape changes depending on the intensity of the hydrophilicity and hydrophobicity. In our previous paper,[29] we proposed the orientational order parameters as the indices to characterize the micellar shape. Here, we introduce the coordinate system with three principal axes of inertia of each micelle. In this coordinate system, the origin is located at the center-of-mass position of the micelle, the x-axis is the principal axis with the largest moment of inertia and the z-axis is that with the smallest moment of inertia. The orientational order parameters p_x, p_y, and p_z are defined by

$$p_i=\left\langle\frac{3\cos^2\theta_i-1}{2}\right\rangle \quad (i=x,y,z), \tag{5}$$

where θ_i is the angle between the vector along the molecular axis of an amphiphilic molecule and the i-axis $(i=x,y,z)$, and $\langle\cdots\rangle$ denotes the average over all amphiphilic molecules.[31] Note that the average is taken for the amphiphilic molecules in the vicinity of the center-of-mass position of the micelle, that is, those in the region of $-\Delta r<x,y,z<\Delta r$. We set $\Delta r=2.5\sigma$ in the calculation of p_i. Ideally, the orientational order parameters take the following values: $(p_x,p_y,p_z)=(1,-0.5,-0.5)$ for a disk, $(p_x,p_y,p_z)=(0,0,-0.5)$ for a cylinder, and $(p_x,p_y,p_z)=(0,0,0)$ for a sphere. It is found from the detailed analysis of the distribution functions of these orientational order parameters that, in practice, three types of micellar shapes are clearly distinguishable by the orientational order parameters: $0.5<p_x<1.0$ and $-0.5<p_y,p_z<-0.25$ for a disk micelle, $-0.25<p_x,p_y<0.5$ and $-0.5<p_z<-0.25$ for a cylindrical micelle, and $-0.25<p_x,p_y,p_z<0.5$ for a spherical micelle.[29] We now calculate the fraction of each micellar shape on the basis of the above-mentioned orientational order parameters. In Figs.

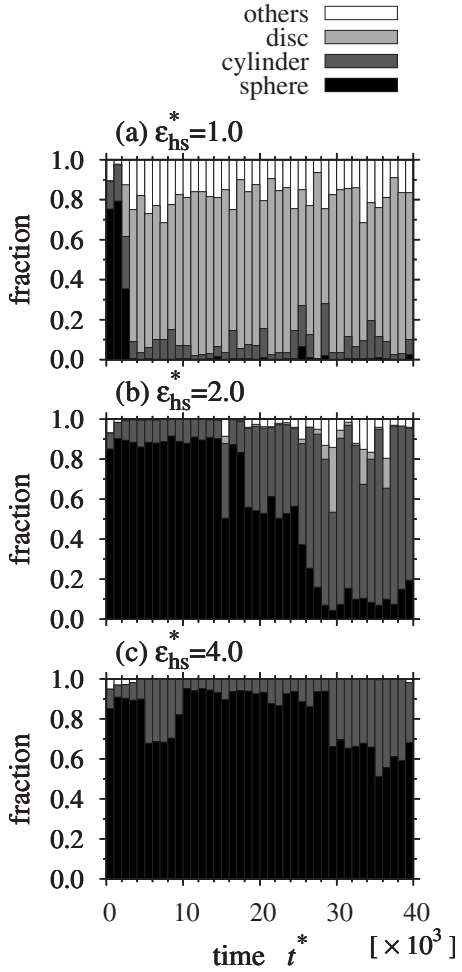

FIG. 7. The fraction of various micellar shapes (disk, cylinder, sphere, and others) of all micelles versus time t in the case of $\varepsilon^*_{SC}=1.0$ (a) for $\varepsilon^*_{hs}=1.0$, (b) for $\varepsilon^*_{hs}=2.0$, and (c) for $\varepsilon^*_{hs}=4.0$. The figures are shown as histograms. The classification of micellar shapes is based on the orientational order parameters concerning the principal axes of inertia of the micelle (Ref. 29).

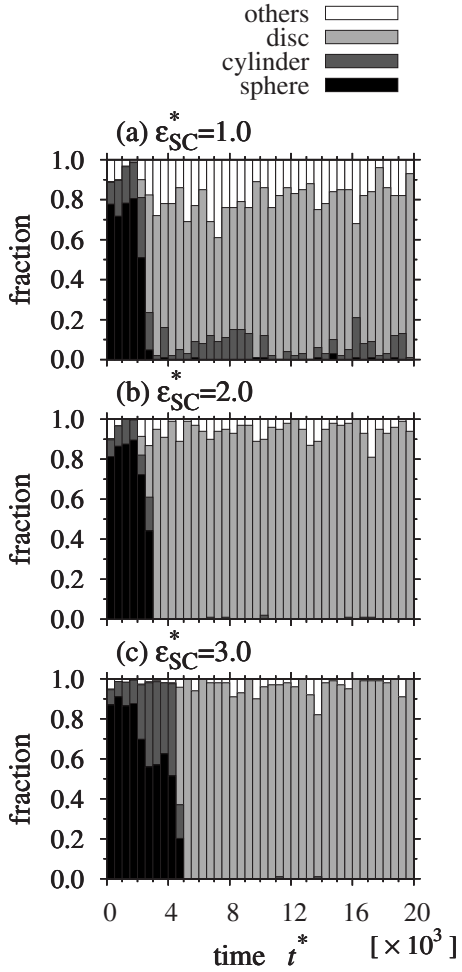

FIG. 8. The fraction of various micellar shapes (disk, cylinder, sphere, and others) of all micelles vs time t in the case of $\varepsilon^*_{hs}=1.0$ (a) for $\varepsilon^*_{SC}=1.0$, (b) for $\varepsilon^*_{SC}=2.0$, and (c) for $\varepsilon^*_{SC}=3.0$. The figures are shown as histograms. The classification of micellar shapes is based on the orientational order parameters concerning the principal axes of inertia of the micelle (Ref. 29).

7 and 8, the time dependence of the fraction of various micellar shapes (disk, cylinder, sphere, and others) of all micelles is presented as histograms for $\varepsilon^*_{SC}=1.0$ and $\varepsilon^*_{hs}=1.0$, respectively. The following characteristic features are found from these figures. (i) The spherical micelles are dominant in the course of the initial micelle formation process [Figs. 7 and 8]. (ii) For $\varepsilon^*_{hs}=1.0$, the disk micelle is dominant after an isolated micelle is formed [Figs. 7(a) and 8]. The fraction of the disk micelles becomes larger as the intensity of the hydrophobicity (ε^*_{SC}) increases [Fig. 8]. (iii) In the case of $(\varepsilon^*_{SC},\varepsilon^*_{hs})=(1.0,2.0)$, the dominant micellar shape is a cylinder after an isolated micelle is formed ($t^*\gtrsim 3.0\times 10^4$) [Fig. 7(b)]. (iv) For $(\varepsilon^*_{SC},\varepsilon^*_{hs})=(1.0,4.0)$, the dominant micellar shape is a sphere although the alternative changes are observed in the fraction of micellar shapes due to the coalescence and fragmentation of micelles [Fig. 7(c)]. This alternation can be a precursor of the dynamic coexistence discussed below (Sec. III B).

B. Dynamic coexistence

In Sec. III A, it was shown that, in the case of $\varepsilon^*_{SC}=1.0$, the dominant micellar shape is a disk for $\varepsilon^*_{hs}=1.0$, a cylinder for $\varepsilon^*_{hs}=2.0$, and a sphere for $\varepsilon^*_{hs}=4.0$. Here, we study the micellar shapes observed in each intermediate parameter range in the case of $\varepsilon^*_{SC}=1.0$: $1.0<\varepsilon^*_{hs}<2.0$ or $2.0<\varepsilon^*_{hs}<4.0$. At first, the snapshots of the micelle formed at various times ($t^*=22\,000$, 24 000, 31 500, and 34 500) are shown in Fig. 9 for $(\varepsilon^*_{SC},\varepsilon^*_{hs})=(1.0,1.5)$. This figure tells us that the micellar shape becomes a disk [Figs. 9(a) and 9(c)] or a cylinder [Figs. 9(b) and 9(d)] as the time elapses. Note that, in the case of $\varepsilon^*_{SC}=1.0$, the dominant micellar shape for $\varepsilon^*_{hs}=1.0$ is a disk and that for $\varepsilon^*_{hs}=2.0$ is a cylinder [Figs. 7(a) and 7(b)]. We then show, in Fig. 10, the snapshots of the micelle formed at various times ($t^*=13\,000$, 14 000, 24 500, and 39 000) for $(\varepsilon^*_{SC},\varepsilon^*_{hs})=(1.0,3.0)$. It is found from this figure that the micellar shape alternates between a cylinder [Figs. 10(a) and 10(c)] and a sphere [Figs. 10(b) and 10(d)]. It must also be noted that, in the case of $\varepsilon^*_{SC}=1.0$, the dominant micellar shape for $\varepsilon^*_{hs}=2.0$ is a cylinder and that for $\varepsilon^*_{hs}=4.0$ is a sphere [Figs. 7(b) and 7(c)]. Both of these figures indicate that two kinds of micellar shapes coexist dynamically.

Hereafter, we investigate the dynamic coexistence of micellar shapes in detail. We show, in Figs. 11 and 12, the time dependence of the total potential energy E_{pot}, the radius of

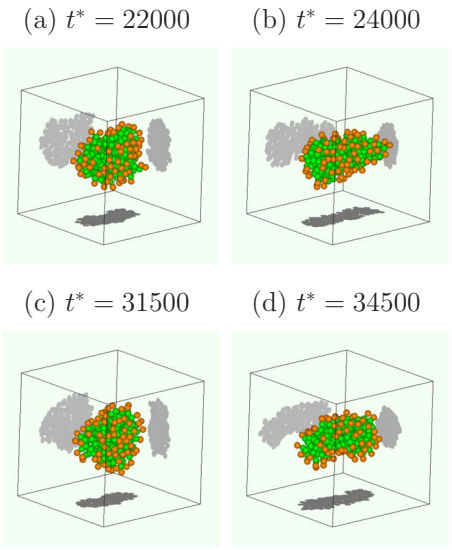

FIG. 9. (Color online) Dynamic coexistence of a disk micelle and a cylindrical micelle for $(\varepsilon^*_{SC}, \varepsilon^*_{hs})=(1.0, 1.5)$: (a) $t^*=22\,000$ (disk), (b) $t^*=24\,000$ (cylinder), (c) $t^*=31\,500$ (disk), and (d) $t^*=34\,500$ (cylinder). Dark gray (or orange color) and light gray (or green color) particles denote hydrophilic head particles and hydrophobic tail particles, respectively. Gray shadows of the amphiphilic molecules projected on three planes are also depicted to make the micellar shape understandable. Note that solvent molecules are not displayed for clarity.

gyration R_g of the largest micelle, the number of micelles n_m, and the fraction of micellar shapes of the largest micelle for $(\varepsilon^*_{SC}, \varepsilon^*_{hs})=(1.0, 1.5)$ and $(\varepsilon^*_{SC}, \varepsilon^*_{hs})=(1.0, 3.0)$, respectively. Figure 11 indicates the following features: (i) The stepwise changes in E_{pot}, R_g, and n_m are observed until a single micelle is finally formed through the coalescence of smaller micelles ($t^* \lesssim 12\,000$). (ii) After the single micelle is formed ($t^* \gtrsim 12\,000$), E_{pot}, R_g, and n_m are almost steady whereas the

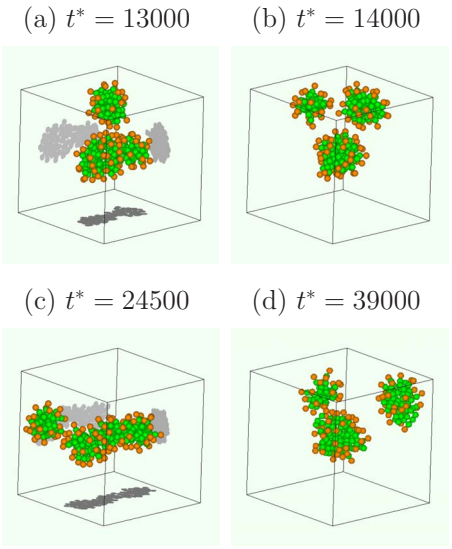

FIG. 10. (Color online) Dynamic coexistence of a cylindrical micelle and spherical micelles for $(\varepsilon^*_{SC}, \varepsilon^*_{hs})=(1.0, 3.0)$: (a) $t^*=13\,000$ (cylinder), (b) $t^*=14\,000$ (sphere), (c) $t^*=24\,500$ (cylinder), and (d) $t^*=39\,000$ (sphere). Dark gray (or orange color) and light gray (or green color) particles denote hydrophilic head particles and hydrophobic tail particles, respectively. Gray shadows of the cylindrical micelles projected on three planes are also depicted to make the micellar shape understandable. Note that solvent molecules are not displayed for clarity.

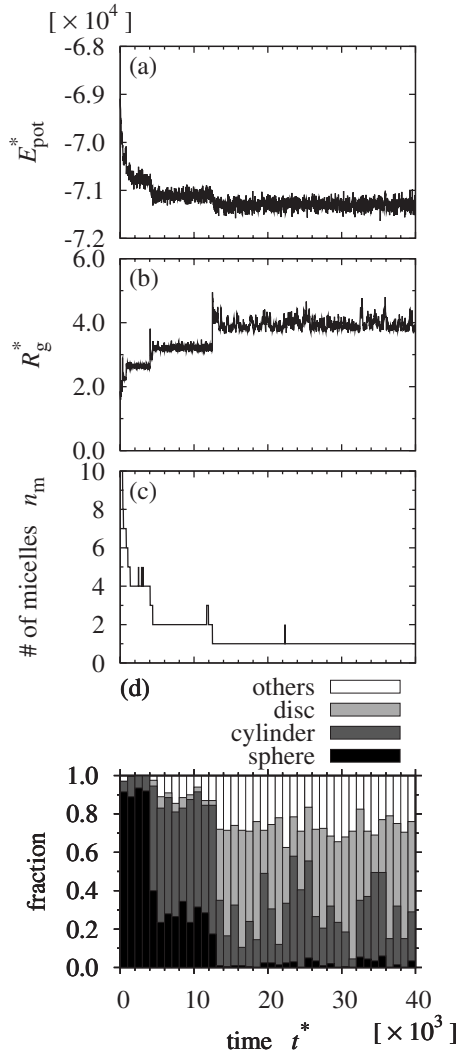

FIG. 11. The time evolution of (a) the total potential energy E_{pot}, (b) the radius of gyration R_g of the largest micelle, (c) the number of micelles n_m, and (d) the fraction of various micellar shapes of the largest micelle in the case of $(\varepsilon^*_{SC}, \varepsilon^*_{hs})=(1.0, 1.5)$.

dominant micellar shape frequently alternates between a disk and a cylinder as depicted in Fig. 9. (iii) The fraction of other micellar shapes which are not classified into three kinds of micellar shapes (disk, cylinder, and sphere) is relatively large especially after the single micelle is formed ($t^* \gtrsim 12\,000$). The reason for this observation is that since no coalescence and fragmentation of micelles occurs at $t^* \gtrsim 12\,000$, the micellar shape change between a disk and a cylinder is the continuous one rather than the alternation between them, which results in the relative large fraction of the intermediate shapes between them. We find from Fig. 12 that after the initial micelle formation ($t^* \gtrsim 4000$), E_{pot} remains almost steady, the sharp increases or decreases of R_g occur repeatedly, and n_m fluctuates between 1 and 3. The fluctuation of n_m implies that the coalescence and fragmentation of micelles occur frequently at $t^* \gtrsim 4000$. It is also found from Fig. 12(d) that the dominant micellar shape alternates between a cylinder and a sphere several times after the initial micelle formation ($t^* \gtrsim 4000$) as shown in Fig. 10. By making a comparison between the time evolution of R_g [Fig. 12(b)], that of n_m [Fig. 12(c)], and that of the fraction of micellar shapes for

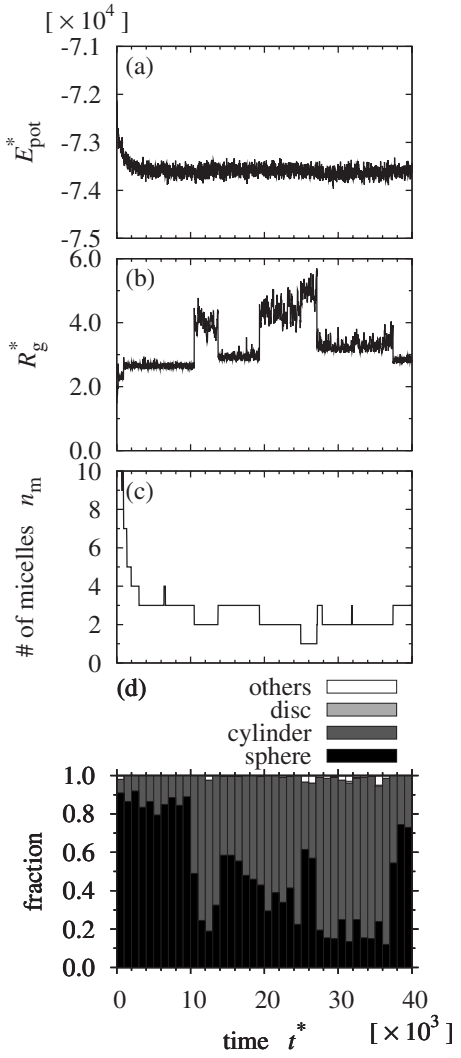

FIG. 12. The time evolution of (a) the total potential energy E_{pot}, (b) the radius of gyration R_g of the largest micelle, (c) the number of micelles n_m, and (d) the fraction of various micellar shapes of the largest micelle in the case of $(\varepsilon^*_{SC}, \varepsilon^*_{hs})=(1.0, 3.0)$.

the largest micelle [Fig. 12(d)], it is clearly found that R_g and the micellar shapes change in association with the coalescence and fragmentation of micelles.

IV. CONCLUSIONS

In conclusion, we have obtained the following new results by carrying out MD simulations of coarse-grained rigid amphiphilic molecules with explicit solvent molecules. (1) Three kinds of isolated micelles (disk, cylindrical, and spherical micelles) are formed at a lower temperature by quenching from a random configuration of amphiphilic molecules in solution at a higher temperature. (2) As the hydrophilic interaction increases, the micellar shape changes from a disk into a cylinder, and then into a sphere. (3) The micellar shape, on the other hand, is not so sensitive to the variation of the hydrophobic interaction. (4) The relaxation of the total potential energies proceeds *in a stepwise manner* and the degree of the stepwise nature is enhanced as the intensity of the hydrophilicity decreases or that of the hydrophobicity increases. (5) The dynamic coexistence of a cylindrical micelle and a spherical micelle accompanies the coalescence and fragmentation of micelles whereas that of a disk micelle and a cylindrical micelle does not, but exhibits the continuous change between them.

Here we discuss the relationship between the second result and the argument by Mitchell *et al.*[32] They illustrated that the micellar shape changes from a disk (bilayer) into a cylinder (rod), and then into a sphere as the curvature of the tail-solvent interface (interfacial curvature) increases (Fig. 2 in Ref. 32). Considering that the interfacial curvature tends to increase as ε_{SC} decreases or ε_{hs} increases as in Fig. 1, the second result is in agreement with the illustration by Mitchell *et al.* in Ref. 32.

The second and third observations lead to the conclusion that the hydrophilic interaction plays an important roll in determining the micellar shape in the interaction parameter range we used. The fourth result can be explained by the following simple argument. The energy gain due to the coalescence of micelles is considered to be large since the cohesive energy by amphiphilic molecules increases as the hydrophilicity decreases or the hydrophobicity increases. Therefore, the energy difference between before and after the coalescence of micelles can be larger as the intensity of the hydrophilicity decreases or that of the hydrophobicity increases.

It is worth mentioning the universal nature of the nonequilibrium dynamics. The stepwise energy relaxation is observed not only in amphiphilic systems but also in chain molecular systems[33–38] and in plasma systems[39] when a system is driven far from equilibrium. In chain molecular systems, the orientationally ordered structure of polymer chains or chain molecules is formed at a lower temperature by quenching from a random configuration at a higher temperature and its growth proceeds in a stepwise fashion.[33–38] In the case of plasma systems, the magnetic energy relaxes into a self-organized state in a stepwise manner when the system is initially excited into a nonequilibrium state.[39] Moreover, the dynamic coexistence of the orientationally ordered state and the randomly oriented state is observed at a certain temperature in polymeric systems.[37] We believe that these two findings, the stepwise energy relaxation and the dynamic coexistence, will provide a key to the research on the universality of the nonequilibrium dynamics.

We now refer to the characterization of micellar shapes. In this paper, we classified the micellar shapes into disk, cylinder, sphere, and others, on the basis of the orientational order parameters concerning the principal axes of inertia of a micelle. Such characterization of the micellar shapes may be appropriate for small micelles,[29] but its validity for large micelles is not obvious because our classification is based on the local information around the center-of-mass position of the micelle. The characterization of large micelles such as threadlike micelles can be seen in Ref. 19.

In a subsequent paper, we will study the molecular mobility and the micellar shape change in amphiphilic solution.[26] For future works, we will analyze the dynamic coexistence from a point of view of free energy. Furthermore, we will carry out MD simulations of semiflexible amphiphilic molecules in solution in order to investigate the

effect of chain rigidity on the micellar shape and the formation processes of micelles and mesophases systematically. We expect that the rigid amphiphilic molecules would favor the formation of disks while the flexible tails would be able to pack more easily into cylindrical or spherical micelles. The preliminary simulation results on semiflexible amphiphilic molecules seem to lend support to this expectation, that is, the micellar shape changes from a cylinder to a disk as the chain rigidity increases.

ACKNOWLEDGMENTS

This work was partially supported by Inamori Foundation and Grants-in-Aid (Nos. 15740262 and 19031019) from the Ministry of Education, Culture, Sports, Science and Technology, Japan. This work was performed with the support and under the auspices of the NIFS Collaborative Research Program (No. NIFS07KDAN002). One of the authors (S.F.) would like to thank Dr. H. Nakamura for his helpful advice on Gaussian splatting techniques.

[1] *Micelles, Membranes, Microemulsions, and Monolayers*, edited by W. M. Gelbart, A. Ben-Shaul, and D. Roux (Springer-Verlag, New York, 1994), pp. 1–104.
[2] J. N. Israelachvili, *Intermolecular and Surface Forces*, 2nd ed. (Academic, London, 1992).
[3] I. W. Hamley, *Introduction to Soft Matter* (Wiley, Chichester, 2000).
[4] H. Matsui, S. Pan, B. Gologan, and S. H. Jonas, J. Phys. Chem. B **104**, 9576 (2000).
[5] T. M. Weiss, T. Narayanan, C. Wolf, M. Gradzielski, P. Panine, S. Finet, and W. I. Helsby, Phys. Rev. Lett. **94**, 038303 (2005).
[6] B. Smit, P. A. J. Hilbers, K. Esselink, L. A. M. Rupert, N. M. van Os, and A. G. Schlijper, Nature (London) **348**, 624 (1990).
[7] B. Smit, P. A. J. Hilbers, K. Esselink, L. A. M. Rupert, N. M. van Os, and A. G. Schlijper, J. Phys. Chem. **95**, 6361 (1991).
[8] P. H. Nelson, G. C. Rutledge, and T. A. Hatton, J. Chem. Phys. **107**, 10777 (1997).
[9] M. Kenward and M. D. Whitmore, J. Chem. Phys. **116**, 3455 (2002).
[10] R. Goetz and R. Lipowsky, J. Chem. Phys. **108**, 7397 (1998).
[11] R. Goetz, G. Gompper, and R. Lipowsky, Phys. Rev. Lett. **82**, 221 (1999).
[12] S. J. Marrink, D. P. Tieleman, and A. E. Mark, J. Phys. Chem. B **104**, 12165 (2000).
[13] H. Noguchi and M. Takasu, Phys. Rev. E **64**, 041913 (2001).
[14] H. Noguchi and M. Takasu, J. Chem. Phys. **115**, 9547 (2001).
[15] M. J. Stevens, J. H. Hoh, and T. B. Woolf, Phys. Rev. Lett. **91**, 188102 (2003).
[16] S. Jury, P. Bladon, M. Cates, S. Krishna, M. Hagen, N. Ruddock, and P. Warren, Phys. Chem. Chem. Phys. **1**, 2051 (1999).
[17] H. Nakamura, Mol. Simul. **30**, 941 (2004).
[18] S. Yamamoto and S. Hyodo, J. Chem. Phys. **118**, 7937 (2003).
[19] N. Arai, K. Yasuoka, and Y. Masubuchi, J. Chem. Phys. **126**, 244905 (2007).
[20] G. Srinivas, D. E. Discher, and M. L. Klein, Nature Mater. **3**, 638 (2004).
[21] S. O. Nielsen, G. Srinivas, C. F. Lopez, and M. L. Klein, Phys. Rev. Lett. **94**, 228301 (2005).
[22] W. Shinoda, R. Devane, and M. L. Klein, Mol. Simul. **33**, 27 (2007).
[23] H. Noguchi and G. Gompper, J. Chem. Phys. **125**, 164908 (2006).
[24] R. Pool and P. Bolhuis, J. Chem. Phys. **126**, 244703 (2007).
[25] G. Mohan and D. I. Kopelevich, J. Chem. Phys. **128**, 044905 (2008).
[26] S. Fujiwara, T. Itoh, and M. Hashimoto, J. Chem. Phys. (unpublished).
[27] C. Tanford, *The Hydrophobic Effect*, 2nd ed. (Wiley, New York, 1980).
[28] S. Fujiwara, M. Hashimoto, and T. Itoh, J. Plasma Phys. **72**, 1011 (2006).
[29] S. Fujiwara, T. Itoh, M. Hashimoto, and Y. Tamura, Mol. Simul. **33**, 115 (2007).
[30] M. P. Allen and D. J. S. Tildesley, *Computer Simulation of Liquids* (Clarendon, Oxford, 1987).
[31] In the case of flexible or semiflexible amphiphilic molecules, the principal axis with the smallest moment of inertia of an amphiphilic molecule can be used as its molecular axis.
[32] D. J. Mitchell, G. J. T. Tiddy, L. Waring, T. Bostock, and M. P. McDonald, J. Chem. Soc., Faraday Trans. 1 **79**, 975 (1983).
[33] S. Fujiwara and T. Sato, Phys. Rev. Lett. **80**, 991 (1998).
[34] S. Fujiwara and T. Sato, Mol. Simul. **21**, 271 (1999).
[35] S. Fujiwara and T. Sato, J. Plasma Fusion Res. **2**, 498 (1999).
[36] S. Fujiwara and T. Sato, J. Chem. Phys. **114**, 6455 (2001).
[37] S. Fujiwara and T. Sato, Comput. Phys. Commun. **142**, 123 (2001).
[38] S. Fujiwara, M. Hashimoto, T. Itoh, and H. Nakamura, J. Phys. Soc. Jpn. **75**, 024605 (2006).
[39] S. P. Zhu, R. Horiuchi, and T. Sato, Phys. Rev. E **51**, 6047 (1995).